Probability Mass Function of Energy for Light-Collecting Surfaces in Rough Geometries and Its Applications in Urban Energy and Photovoltaics

Ziar, Hesan

DOI
10.1109/JPHOTOV.2025.3558270

Publication date
2025

Document Version
Final published version

Published in
IEEE Journal of Photovoltaics

Probability Mass Function of Energy for Light-Collecting Surfaces in Rough Geometries and Its Applications in Urban Energy and Photovoltaics

Hesan Ziar, *Senior Member, IEEE*

***Abstract*—Sunlight throughout urban areas largely impacts local climate [sustainable development goal (SDG) 13], residents' well-being (SDG 3), and access to clean energy (SDG 7). However, sunlight availability on various urban surfaces is affected by urban geometry. Here, in this work, a probabilistic framework to evaluate the interplay between sunlight and urban geometry is presented, and its immediate applications in urban energy studies are demonstrated. A probability mass function that predicts the energy production of a group of light-collecting surfaces, such as solar photovoltaic (PV) systems, installed in rough geometries, such as urban areas, is derived. Along the way, an expression for the sky view factor (SVF) is formulated within rough geometries as well as a link between the capacity factor of the residential PV fleet and urban geometry. The predictions of the mathematical framework are validated using the digital surface model and collected PV systems data in The Netherlands. This work primarily helps understand the underlying relation between the geometrical parameters of a rough surface and the received sunlight energy on a subset of that surface. Exemplified applications are swift SVF calculations and residential PV fleet yield predictions, which, respectively, support efficient urban energy assessments and privacy-preserving electrical grid management.**

***Index Terms*—Digital surface model (DSM), LiDAR, photovoltaics (PVs), probability distribution function (PDF), sky view factor (SVF), solar energy, urban geometry.**

I. Introduction

SUNLIGHT is the driving force for life on earth [1]. It is the origin of almost all energy resources, and its interaction with the earth's atmosphere determines the climate [2]. More than half of the world's population is currently living in urban areas and is expected to rise to more than two-thirds by 2050 [3]. The physical and mental health, clean energy access, and climate that urban residents experience are linked to sunlight access, which marks three of the United Nations' sustainable development goals [4]. Sunlight in urban areas, or generally stated light on rough surfaces, is a *function* of its geometrical features. However, how does this function look like, given the intermittency of sunlight and randomness of urban morphology? When the answer to this question is known, several application-oriented questions concerning sunlight in urban areas can be answered subsequently. Solar photovoltaic (PV) yield prediction and grid management, sunlight access of urban dwellers and health assessment, and the heat island effect and urban planning are a few example application areas that will largely benefit [5], [6], [7], [8], [9], [10], [11], [12], [13].

There are already valuable research works hinting toward an answer, but a clear comprehensive understanding is lacking. The result from precise physics-based 2-D/3-D simulations backed up with powerful PCs [14], [15], [16] holds for a confined and small-size geometry within an urban environment, thus remaining case dependent [17], [18], [19], [20] and failing to provide a thorough understanding. Simplified synthetic models, on the other hand, lack temporal resolution, cannot be applied to a tailored subset of urban surfaces, and work based on curve-fitted coefficients that have limited physical meaning [21], [22]. Moreover, with the help of artificial intelligence, research has been done to find correlations between rough surface geometrical indicators (such as building density and height, building footprints, building height and volume variance, etc.) and access to sunlight [23], [24], [25], [26]. Despite such studies covering broader ranges of cities, the true interplay between geometry and sunlight access remains in a closed box of artificial intelligence algorithms. Furthermore, when it comes to applying such solutions to a certain application, i.e., PV system yields, detailed information from each PV system (i.e., light-collecting surface) is demanded, which, in reality, conflicts with the privacy and preference of residential PV system owners [27], [28]. Besides, the trained machine learning models based on, for instance, residential PV system data, can become obsolete when PV systems are installed at a fast pace in urban environments [29]. In such situations, probabilistic solutions can provide valuable insights and understanding.

Within this study, this fundamental question is approached from a different angle, by considering it as a problem of an ensemble of systems, i.e., a fleet of light receivers (e.g., PV systems). Using this feature, surfaces in an urban area can be treated not individually but as a large group. Such a perspective also lays the ground for tackling privacy concerns or data limitation issues as utilizing group-level information can keep the individual data unknown or very coarse to track down. The rule of the large numbers will then apply, and predictions can be made using

Received 10 September 2024; revised 3 March 2025; accepted 1 April 2025. Date of publication 21 April 2025; date of current version 20 June 2025.

The author is with the Photovoltaic Materials and Devices Group, Department of Electrical Sustainable Energy, Faculty of Electrical Engineering, Mathematics, and Computer Science, Delft University of Technology, 2628 Delft, The Netherlands (e-mail: h.ziar@tudelft.nl).

This article has supplementary downloadable material available at https://doi.org/10.1109/JPHOTOV.2025.3558270, provided by the author and contains the derivation of the presented equations.

Digital Object Identifier 10.1109/JPHOTOV.2025.3558270

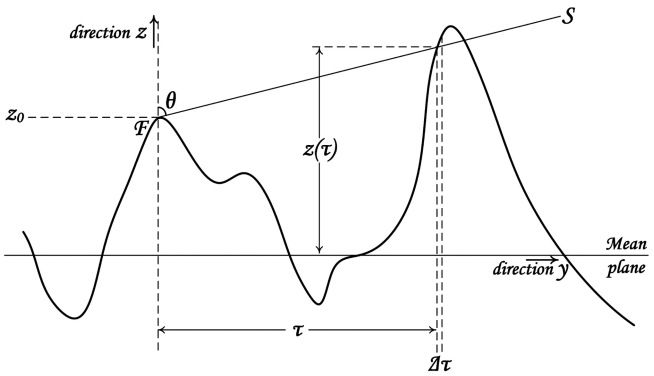

Fig. 1. Illustration of a section of a randomly rough surface illuminated by a source at point *S*.

probability and statistics. Applying probability law enables tackling the problem of geometrical randomness and facilitates the analytical formulation of the target function. The prime goal is to extract the probability distribution of expected sunlight energy in an urban area, characterized by its geometry, for a specific time instant or duration. Following that, it is convenient to make several parametric sensitivity analyses to understand better the interplay between an urban area's geometry and its sunlight access. When the target probability distribution is well extracted and characterized, several applications can be explored. Here, applications via PV power production are demonstrated without the need for detailed information on the systems' exact location and characteristics (privacy preserving).

The rest of this article begins with presenting the mathematical framework. Next, the general formulation for the probability distribution function (PDF) of expected sunlight access to a fleet of urban light-collecting surfaces is extracted. Then, the findings are visualized by introducing parametric graphs. Furthermore, to assess the mathematical formulation, a study is run using real data from residential PV systems in The Netherlands. Finally, the impacts are highlighted, and a conclusion is made.

II. Extending Wagner–Smith Shadowing Theory

Let us consider a random profile, as depicted in Fig. 1. It is interesting to know the probability that point *F*, with a vertical distance of z_0 from the mean plane and local slopes of p_0 and q_0 in the *x*- and *y*-directions, is not shaded. Point *F* intersects line SF, the line that shows the direction of direct light toward the target plane, with angle θ. Let us call this probability *S*, which is a function of z_0, p_0, q_0, and θ. Since z_0, p_0, and q_0 are the parameters of point *F* and all the points on the right-hand side of point *F* can potentially cause a shadow, the probability *S* can be written as

$$S(z_0, p_0, q_0, \theta) = S(F, \theta) = \lim_{\tau \to \infty} S(F, \theta, \tau). \tag{1}$$

It is assumed that roughness within the target plane is isotropic. This means that the azimuth of the light source does not influence the analysis.

The differential equation describing the shadowing of such a random profile can be found as [30], [31]

$$\frac{\partial S(\tau)}{\partial \tau} = -S(\tau) g(\tau). \tag{2}$$

$g(\tau)$ is the probability density function of the random variable that gives the probability that the line SF intersects with the profile in $(\tau,\tau+\Delta\tau)$, while the line has not crossed the profile in $(0,\tau)$. The general form of solution to this differential equation is

$$S(\tau) = h(\mu - q_0) \exp\left(\int_0^{\infty} -g(\tau)\, d\tau \right) \tag{3}$$

where μ is $\cot\theta$ at point *F*, and *h* is the Heaviside step function. The key here is to evaluate $g(\tau)$. Smith [31] evaluated $g(\tau)$ using $f_{ZQ}(z,q|F,\tau)$ as the joint probability density function of heights and slopes at $y = \tau$, conditional upon the height and slope at $y = 0$ (point *F*), and obtained

$$g(\tau)\Delta\tau = \frac{\Delta\tau \int_{\mu}^{+\infty} (q-\mu) f_{ZQ}(z, q|F, \tau)\,|_{z=z_0+\mu\tau}\, dq}{\int_{-\infty}^{+\infty} dq \int_{-\infty}^{z_0+\mu\tau} f_{ZQ}(z, q|F, \tau)\, dz} \tag{4}$$

where $\Delta\tau$ can be canceled out from the two sides. Now that $g(\tau)$ is known, plugging (4) into (3) gives the probability that a point on the surface is not shaded. It is noted that the reason that $g(\tau)$ and consequently $S(\tau)$ are not dependent on *p* is that the profile roughness was assumed to be isotropic.

When the probability distribution of the points on a profile is known, (4) can be evaluated. Smith [31] evaluated the case that the PDFs of slopes and heights are normal and obtained a close formula for $S(\tau)$. Here, a general form for the solution to the differential (2) is desired, regardless of the type of distribution for heights and slopes. If such a solution is found, it can help with understanding and implementing shadowing theory for several applications, including urban energy and PVs.

Assuming that slope and height, as the random variables of an isotropic surface profile, are independent, one can work out (4) while taking advantage of the PDF, cumulative distribution function (CDF), and mean function to obtain the solution to (2) as

$$S(\tau) = S(F, \theta, \tau) = h(\mu - q_0)(F_Z(z = z_0))^{\Lambda(\mu)} \tag{5}$$

where

$$\Lambda(\mu) = \frac{E(q \geq \mu)}{\mu} - (1 - F_Q(q = \mu)). \tag{6}$$

F_X denotes the CDF of the random variable *X*, and *E* denotes the expected value function. Equation (5) has four interesting special cases. The first special case is when the height of point *F* is very high, which increases the possibility of being illuminated. It can be seen that

$$\lim_{z_0 \to \infty} S(\tau) = h(\mu - q_0) \tag{7}$$

which equals one for $\mu \geq q_0$. This makes sense because, when the height of the point increases, the chance of being illuminated must also increase. For large heights, this chance approaches unity as long as the local slope at that height is smaller than the

light ray's slope ($\mu \geq q_0$). The second special case is when the point is located in a valley. Then, one has

$$\lim_{z_0 \to -\infty} S(\tau) = 0. \tag{8}$$

This is reasonable, as valleys are mostly in the shade; the deeper the valley, the less chance for illumination. The third special case is when the light source is high in the sky and directly shining from above. This happens when $\mu = \cot\theta \to \infty$. This leads to $\Lambda(\mu) = 0$. It can be written that

$$\lim_{\mu \to \infty} S(\tau) = 1. \tag{9}$$

The fourth case is when the light source is at the horizon, meaning that $\mu = \cot\theta \to 0$. Thus

$$\lim_{\mu \to 0} S(\tau) = 0. \tag{10}$$

This is aligned with the observation that as the sun goes down on the horizon, all places get shaded, but the ones with negative local slope and very high local height ($0 \geq q_0$ and $z_{0\to\infty}$).

So far, an expression for $S(z_0,p_0,q_0,\theta) = s(\tau,\theta)$ has been obtained, whose value is different per location on the profile. To have an expression for the whole profile that is independent of local height and slope, $S(\theta)$, the law of the unconscious statistician is used, which is $E[g(x)] = \int g(x) f_X(x) dx$. This expression can be written as

$$S(\theta) = \int_{-\infty}^{+\infty} dz_0 \int_{-\infty}^{+\infty} dp_0 \int_{-\infty}^{+\infty} dq_0 S(z_0, p_0, q_0, \theta) \times f_Z(z_0) f_P(p_0) f_Q(q_0) \tag{11}$$

where f_X is the PDF of the variable X. With a few mathematical steps, one will end up with the following equation:

$$S(\theta) = F_Q(q_0 = \mu) \left(\frac{1}{\Lambda(\mu) + 1} \right). \tag{12}$$

Equation (12) is the general answer to the "What is the chance of illumination for a point on a randomly rough surface?" Now that the general form of the solution [(12) and (6)] has been obtained, it is noted that $S(\theta)$ is always equal to or less than unity because it is a multiplication of two positive functions that are always equal to or less than 1. Since several well-known probability density functions have analytical forms for their CDF and expectation expressions, using (12) and (6) will be straightforward. It is noted that it seems no simple closed formula was reported in the literature. Even the generalizations made by Brown [32] and Bourlier et al. [33] ended up in closed formulas that still involve an integration, and the authors missed further explorations such as special cases of these equations and especially expressing them in the forms of mean and CDF functions, which are known for many distributions and are straightforward to use. To do a sanity check on the obtained equations, normal distribution for heights and slopes was considered, and the same results reported in the work of Smith [31] were obtained.

When a profile's height or slope is available, it is possible to obtain $S(\theta)$. To show some examples, a MATLAB code based on the aforementioned formulation was run, and the $S(\theta)$ function for various distributions of profile slopes and profile heights was obtained (see supplementary downloadable material).

Furthermore, to apply the obtained formulation to a real urban-level situation, the digital surface model (DSM) of Delft, in The Netherlands [34], has been used. The DSM data are the height data of all objects on the earth's surface. For this study, the vegetation was removed using the QGIS software. The resolution of data is 0.5 m. The $S(\theta)$ function was obtained for two regions in Delft: the city center and the countryside. As can be seen in Fig. 2, the countryside has a higher chance of illumination at all incoming angles. This is intuitive because higher roughness at the city center makes more shadows, and as a result, the chance of a randomly selected surface being illuminated is less than a surface in the countryside, where the houses are far apart and surrounded by open fields. Furthermore, this result is aligned with previous works in the literature, reporting that inner city areas are more frequently shaded by objects and, as a result, have a lower albedo; thus, the inner city is warmer (or in other words, the sky is more blocked by the objects, and consequently, less heat can be radiated back to the atmosphere).

III. Sky View Factor for a Differential Surface Within a Randomly Rough Profile

The sunlight energy received by a surface in a randomly rough profile not only depends on its illumination chance but also on how much of the sky dome is visible to that surface. It is known as the sky view factor (SVF) and is tightly linked to the diffuse component of sunlight. Therefore, an expression for the SVF in a randomly rough profile needs to be found. To obtain the SVF, it is noted that the SVF from a differential surface is the summation of the view factors from that differential surface to all sky portions. The view factor from a differential surface to a surface is

$$VF_{dA_i \to A_j} = \int_{A_j} \frac{\cos\theta_i \cos\theta_j}{\pi R^2} dA_j. \tag{13}$$

Considering Fig. 3, dA_j can be replaced by $\sin\theta\, d\theta\, d\varphi\, R^2$. Since the line from dA_i is always perpendicular to A_j, then $\cos\theta_j = 1$, and $\cos\theta_i = \cos\theta$. Thus, (13) can be rewritten as

$$VF_{dA_i \to A_j} = \frac{1}{2\pi} \int_{\varphi} \int_{\theta} \sin 2\theta\, d\theta\, d\varphi. \tag{14}$$

For a free sky (case of a smooth surface), this integral is equal to unity. However, due to the roughness of the profile, only some parts of the sky are possible to be observed. The possibility of dA_j being observed is the same as the possibility of dA_i being illuminated by sun rays coming from dA_j. Therefore, the integral is multiplied by the chance of being illuminated, $S(\theta)$, and is integrated over the whole sky dome ($0 < \theta < \pi/2$, $0 < \varphi < 2\pi$) to obtain the SVF. It gives

$$\text{SVF} = \int_0^{\frac{\pi}{2}} S(\theta) \sin 2\theta\, d\theta\,. \tag{15}$$

By plugging (12) into (15), one has

$$\text{SVF} = \int_0^{\frac{\pi}{2}} F_Q(q_0 = \mu) \left(\frac{1}{\Lambda(\mu) + 1} \right) \sin 2\theta\, d\theta\,. \tag{16}$$

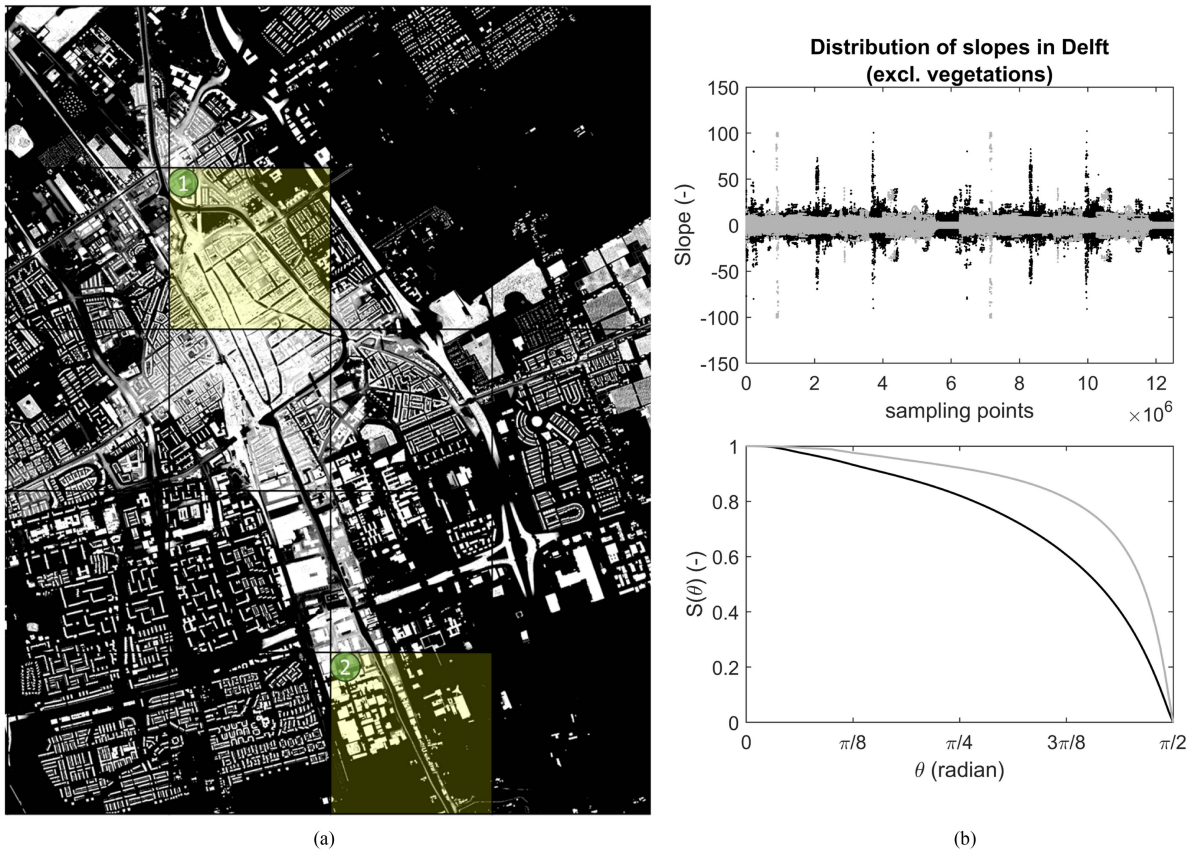

(a) (b)

Fig. 2. (a) DSM of Delft excluding vegetation with a resolution of 0.5 m, where two regions in the city center and countryside are highlighted and coded with numbers 1 and 2, respectively. The brighter the color, the higher the height of the pixel. (b) Slope values on x- and y-directions for the two regions (top). The illumination chance function versus the zenith angle of the light source (bottom). The black points/plot are for the city center, while the gray points/plot are for the countryside.

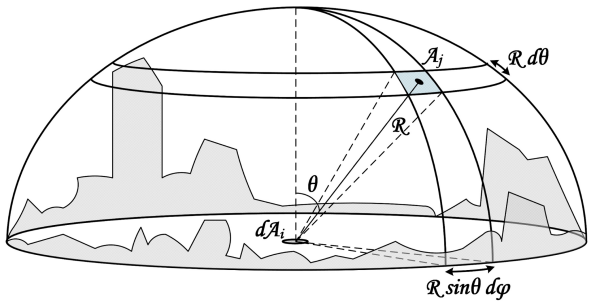

Fig. 3. Illustration of a view factor from a differential surface to a portion of the sky (blue surface). The gray areas represent obstacles blocking parts of the sky dome as a result of a random roughness of the profile (e.g., buildings in urban areas).

Equation (16) gives the SVF for a randomly rough surface. Since the surface is assumed isotropic, it can be seen that the derived SVF formula is independent of φ. It is noted that (16) by itself can have applications in urban energy studies, as the SVF is tightly linked with the heat island effect in urban areas [35]. Not only in urban energy but also wherever automatic feature extraction from digital elevation model is needed, for instance, in geography, geomorphology, cartography, hydrology, glaciology, forestry and disaster management, and relief visualizations, the SVF has applications [36].

Without the need for cumbersome calculation [35] or time-consuming horizon-scanning experiments [36] in many parts of a city, one can obtain the SVF of different neighborhoods of the city by knowing their roughness profiles. Given the importance of the SVF, let us linger a little more on this topic and investigate the validity of our SVF formulation. Three neighborhoods in Delft are selected, namely, city center, suburb, and countryside, each with a size of 1250 $\times$ 1250 m^2. Each neighborhood is divided into 100 equal pieces, and within each piece, the SVF is calculated at every 0.5-m step through two approaches. One is based on accurate horizon scanning and Steyn's formula [37] that is already experimentally validated and used by several research works [38], [39], and the other is the probabilistic approach proposed in the present work. The SVFs obtained from each piece of each neighborhood are averaged, resulting in 100 SVFs for each neighborhood. Fig. 4 shows the comparison between the two methods. As can be seen, the low root-mean-square error (RMSE) and mean bias error (MBE) values ensure the validity and reliability of the proposed probabilistic SVF equation. The positive MBE values suggest slight overestimation, which is expected. That is because when a part of the sky dome is blocked by the surface profile, that part will have zero contribution to the SVF value, while in our formulation, a nonzero probability might be assigned to that point, depending on the distribution of heights and slopes in the surface profile.

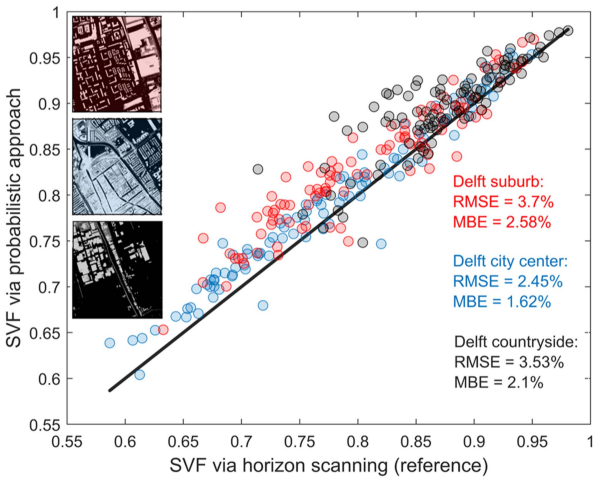

Fig. 4. Assessing the validity of the proposed SVF formulation. Neighborhoods are shown with the same color code as the corresponding data points (suburb: red, city center: blue, and countryside: gray). To obtain the colored data points, 2-D matrices of height and slope profiles were put in one column of data, and then, through (16), the SVF was calculated. The black line shows the reference SVF obtained via horizon scanning. For the horizon scanning approach and its detailed implementation, see [38].

For the three neighborhoods in Delft, the correlation coefficient between the height and slope profiles lies within $|r| < 0.02$. The texture aspect ratio (Str), a measure of surface isotropy, is in the range of $0.08 < \text{Str} < 0.12$ for the neighborhoods. Delft and later Eindhoven that are looked into in this article are European cities, which are grown organically over time, making their surface morphology more isotropic. To further evaluate the impact of the surface isotropy assumption and independency of height and slope profiles on SVF calculations, four planned (not organically grown) cities in the United States were also examined: Washington DC, Irvine, Grand Forks, and Houston. They are, respectively, located in the East, West, North, and South sides of the country. The LiDAR points were obtained from the 3DEP LidarExplorer portal of the U.S. Geological Survey science database [40]. One neighborhood per city is examined for SVF calculations. As shown in Fig. 5, here, it is also observed that the proposed probabilistic SVF formula provides accurate results, supported by low MBE and RMSE values. Similar to Delft's neighborhoods, a slight overestimation is detected. The calculated Str values for the U.S. cities neighborhoods are $0.02 < \text{Str} < 0.07$, while their correlation coefficients are $|r| < 0.003$. Compared with Delft's neighborhoods, they exhibit lower surface isotropy and lower correlation between height and slopes, yet they slightly provide more accurate SVF. It hints that the independence of height and slope profiles might have more influence on the SVF calculation accuracy than the surface isotropy assumption. Yet a thorough statistical study is needed to confirm this guess, which is out of the scope of the present work.

It is noted that the suggested SVF equation drastically reduces the calculation time. To put it into perspective, in our calculations, the SVF based on horizon scanning took almost 100 h for each neighborhood, while for the probabilistic SVF, it was as low as 10 s. It means that, per location, in this study, the proposed probabilistic method is 36 000 times faster. This number is subject to change depending on data point density and horizon scanning radius (i.e., the more points per area and/or the longer scanning radius, the bigger the time advantage).

Besides computational time, the proposed method has data and memory advantages as well. Although the same 3-D information of the city (e.g., LiDAR data) is required for both approaches, the proposed probabilistic method does not need georeferenced data. An XYZ information of a city surface, in any order of arrangement, is sufficient for the probabilistic approach because it does not affect the PDF, CDF, and mean function of the dataset. For the horizon scanning approach, however, the arrangement of data points does influence the outcome because the distance between the observer and an object on the horizon influences the SVF; thus, the data must be georeferenced to ensure an accurate assessment. Moreover, the memory needed to compute is much less in the proposed approach as only a table of XYZ data is required. For horizon scanning, a georeferenced 3-D information of the target area must be kept in the memory while running the calculations.

In the same manner but with more steps, one can work out an expression for the SVF of a tilted surface (with a tilt angle of Υ) placed within a rough geometry, as expressed by the following equation:

$$\text{SVF}_{\gamma} = \left(\frac{1}{2}\right)(1+\cos\gamma)\int_{0}^{\frac{\pi}{2}} S(\theta)\sin 2\theta d\theta. \tag{17}$$

It is noted that for $\Upsilon = 0$, this expression converges to (15).

IV. Probability Mass Function of a Light-Collecting Fleet in Rough Geometries

Now, an urban area with massive implementation of solar PV systems (as an example of light-collecting technology) is considered, with no exact information about the locations of PV systems. This is usually the case where due to the rapid growth of PV system installations, lack of data, or privacy concerns, exact information is not immediately available.

It is assumed that there are n number of PV systems randomly distributed in an urban area. Now, the installation spot of all these PV systems is zoomed in on, one by one. The chance of being sunny for PV systems in this city is $S(\theta)$. Therefore, the probability that α PV systems out of the n PV systems are sunny (P_{α}) can be formulated based on binomial probability, as

$$P_{S(\theta)}(\alpha) = \binom{n}{\alpha} S(\theta)^{\alpha}(1-S(\theta))^{n-\alpha}. \tag{18}$$

When α PV systems out of the n PV systems are sunny, the total solar irradiated power on them is

$$E_{S(\theta)}(\alpha) = \binom{n}{\alpha} S(\theta)^{\alpha}(1-S(\theta))^{n-\alpha}(\alpha\, w_1) + n\, w_2 \tag{19}$$

where w_1 is the solar power from the direct component of sunlight, and w_2 is the same but from the diffuse component of sunlight. w_1 is factored by alpha because only sunny systems receive the direct component of sunlight. All the PV fleet members, whether shaded or sunny, receive the diffuse component. This is

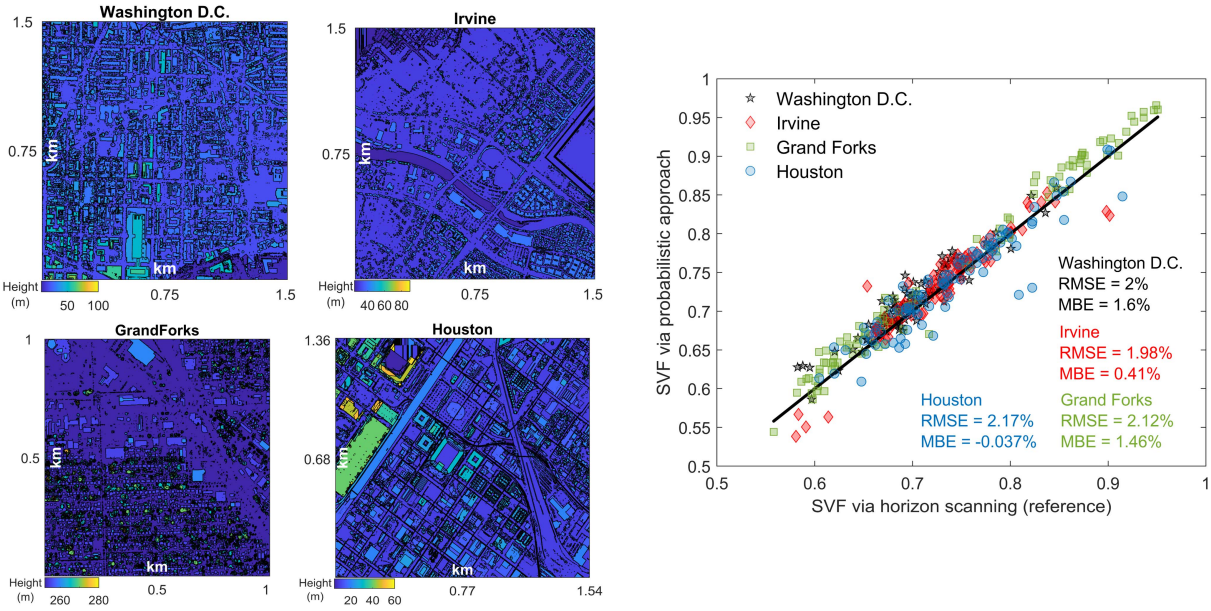

Fig. 5. (Left) contour plots of the four scanned neighborhoods in Washington DC, Irvine, Grand Forks, and Houston for SVF calculation comparison. They are, respectively, 1.5×1.5, 1.5×1.5, 1×1, and 1.33×1.54 km^2 with 1-m resolution. (Right) comparison of SVF calculation via horizon scanning (black line) and the proposed probabilistic framework (scattered points).

why w_2 is multiplied by n. Regardless of the angle of incoming direct sunlight, a PV system, no matter where it is placed, will receive the diffuse part of the light. Therefore, the term nw_2 is not multiplied by the probability mass function (PMF) ($P_{S(\theta)}(\alpha)$) but only added to obtain the mathematical expectation function. w_1 can be obtained by

$$w_1 = I_b \left(\frac{1}{n}\right) \sum_{\gamma=\gamma^-}^{\gamma=\gamma^+} \mathbf{n}_M.\mathbf{n}_S \tag{20}$$

where I_b is the direct component of sunlight (either measured at meteorological stations or extracted from the global horizontal irradiance (GHI) measurement and irradiance decomposition models), and n is the number of light collectors. $\mathbf{n}_M$ and $\mathbf{n}_S$ are, respectively, the unit vectors of the light-collecting surface and the light source. When the azimuth angles of the light collector (A_M) and the light source (A_S) are considered, the scalar multiplication under the summation yields $\sin(\Upsilon)\sin(\theta)\cos(A_M\text{-}A_S) + \cos(\Upsilon)\cos(\theta)$ and when azimuth angles are aligned, it turns into $\cos(\theta\text{-}\ \Upsilon)$. Similar to the previous section, θ is the angle of incidence between the sun rays and the normal to the horizontal plane, and Υ is the tilt angle of the light collector (e.g., PV system), ranging from Υ^- to Υ^+.

Since w_2 is related to the diffuse component, a way to formulate it needs to be found, and it is not as straightforward as w_1. The diffuse component of sunlight falling on a surface is the multiplication of diffuse horizontal irradiance (DHI) and the SVF. This can be written as

$$w_2 = I_d \left(\frac{1}{n}\right) \sum_{\gamma=\gamma^-}^{\gamma=\gamma^+} \mathrm{SVF}_\gamma \tag{21}$$

where I_d can be retrieved from meteorological stations or by breaking down GHI via decomposition models. When all the light collector surfaces have the same tilt, or when an average tilt is considered for all the PV systems due to information limitation, (20) and (21) converge to $w_1 = I_b\cos(\theta\text{-}\Upsilon)$ and $w_2 = I_d\mathrm{SVF}_\Upsilon$, respectively. Summing up the mathematical expectation function from 0 to n will give the expected value of impinging sunlight on a fleet of PV systems installed randomly in a rough geometry

$$E_{S(\theta)} = \sum_{\alpha=0}^{\alpha=n} \left(\binom{n}{\alpha} S(\theta)^\alpha (1 - S(\theta))^{n-\alpha} (\alpha\, w_1) \right) + n\, w_2. \tag{22}$$

Knowing that

$$\sum_{i=0}^{i=n} i \binom{n}{i} p^\alpha (1-p)^{n-\alpha} = np \tag{23}$$

will give

$$E_{S(\theta)} = nS(\theta)w_1 + nw_2. \tag{24}$$

Note that when applying the summation to the expectation equation, nw_2 remains outside ($E[aX + b] = aE[X] + b$). Having (6), (12), (20), (21), (17), and (24), one can calculate the expected value of impinging sunlight energy on a rough surface, such as an urban area, where a large number of light collector surfaces, such as PV systems, are implemented. In the derivation of the PMF, it is assumed that having light collectors would not change the morphology of the surface profile. Multiplying (24) by the average area of the installed PV systems (A) and the sunlight to electricity conversion efficiency (η) will give the expected value of electrical power produced by a fleet of PV systems installed in an urban area

$$P^{\text{elec.}}_{S(\theta)} = E_{S(\theta)} A\, \eta. \tag{25}$$

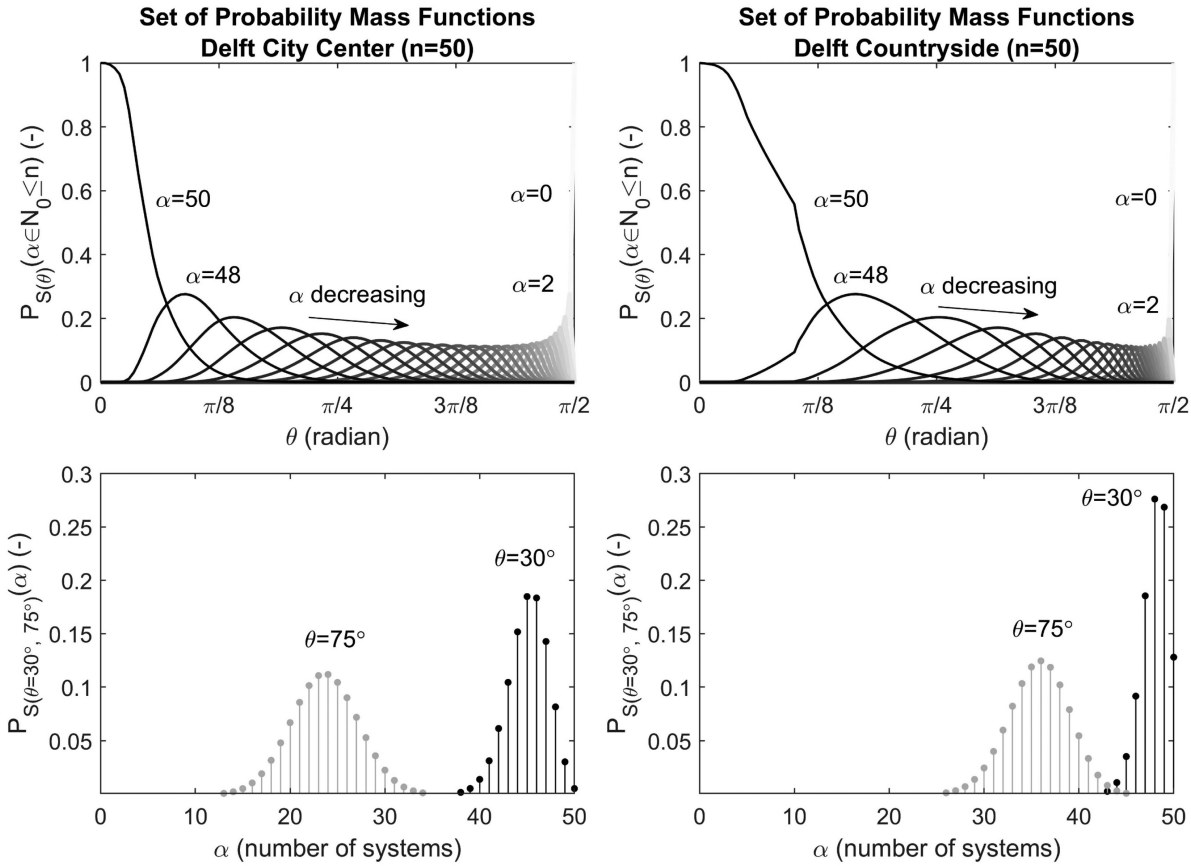

Fig. 6. PMFs for 50 PV systems placed randomly in two regions of Delft (city center and countryside). The top graphs show the PMFs, obtained from (18), for different integer values of α (number of sunny PV systems) while changing the θ (zenith angle of the sun). For every integer value of α, the $P_{S(\theta)}(\alpha)$ function is continuous. For better visualization, as α changes, from one graph to another, the darkness of the graph changes as well. The bottom graphs show PMFs, obtained from (18), for two values of θ (30° and 75°) while changing the integer value of α from 0 to 50. When θ is fixed, the $P_{S(\theta)}(\alpha)$ function is discrete.

The superscript elec. is used to differentiate the symbol of power from probability. At this point, it is interesting and important to visualize the derived mathematical formulations for better understanding. Here, the PMF (18) and the expected value function (19) are visualized for the two regions in the city of Delft. Fig. 6 shows the PMF, $P_{S(\theta)}$, for two hypothetical 50-system PV fleets placed in the city center and countryside of Delft. The purpose of this figure is to visualize the dynamics of the $P_{S(\theta)}$ function under various conditions, namely when the number of sunny PV systems varies at a fixed sun zenith angle (bottom graphs) and when the sun zenith angle changes while the number of sunny PV systems kept fixed (top graphs). Comparing the two bottom graphs in Fig. 6 shows that moving from the countryside to inner city parts flattens and shifts the PMFs. The same happens when θ increases (the sun goes down on the horizon). This is interestingly in line with the previously reported experimental and modeling works [41], [42], [43], [44].

V. Relation Between Urban Environment Geometry and the Capacity Factor of Solar PV Fleets

To investigate the use cases of the aforementioned mathematical formulation, the expected value of electrical power from a hypothetical fleet of 50 PV systems placed in the two regions of Delft (city center and countryside) is plotted in Fig. 7. This graph tells how much power is expected from the fleet without the need

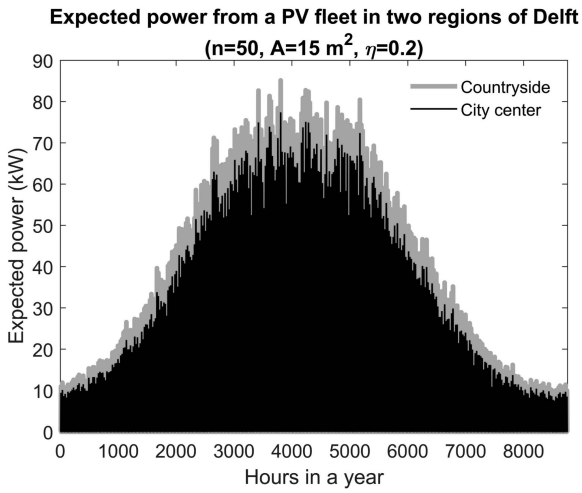

Fig. 7. Expected power from an imaginary fleet of PV systems installed in two different regions of Delft. An average area of 15 m^2 per system and a fixed efficiency of 0.2 were assumed, yielding 150 kW as the fleet's nominal capacity. Data from Meteonorm were used for the direct normal irradiance and the DHI components of light.

for privacy-sensitive information (e.g., details of the PV system, their exact location, etc.) or the need for cumbersome lengthy simulations. The main needed parameter is the total installed capacity of the fleet. An interesting observation is that Fig. 7 hints at how the geometry of the urban environment affects the capacity factor (CF) of PV installations. In this hypothetical example, the yearly CF for the fleet in the city center is 7.54%, while in the countryside, it is 8.64%. The CF is the ratio of the produced energy by an electricity plant to the total amount of energy that the plant could produce if it were running all the time with its rated power capacity. Thermal power plants offer a high CF, while renewable electricity generation, such as solar PV, is bound primarily by the intermittency of the source and then by the deviation of the working criteria from the standard test conditions (STCs). Therefore, for solar PV systems, there are two fundamental factors affecting the CF. First is the day and night cycle that causes the intermittency and then the deviation of ambient conditions from the STC, such as high temperature and low irradiance, that affect the working efficiency of PV cells. Let us name them, respectively, capacity factors for intermittency and working efficiency and show them as CF_i and CF_η. These two fundamental factors are very well formulated in the literature. CF_i is the ratio of equivalent sun hours (ESH) to 24, while CF_η is the ratio of working efficiency under ambient irradiance and temperature conditions (G and T) to the efficiency under STCs. The simplest way to represent them is through $\mathrm{CF}_i = \mathrm{ESH}/24$ and $\mathrm{CF}_\eta = \eta(G, T)/\eta(\mathrm{STC})$. Using the framework introduced in this article, one can formulate the third pillar to the CF of PV systems, which shows that urban areas with rougher geometry fundamentally pose a limit to the CF through less chance of illumination for surfaces. This is mathematically formulated by the expectation function, $E_{(S(\theta))}$. One can write

$$CF_g = \frac{E_{S(\theta)}}{E_{S(\theta)=1}} = \frac{S(\theta)w_1 + w_2}{w_1 + w_2} \tag{26}$$

which is the CF limit imposed by the geometry of the urban area. CF_g can change from $w_2/(w_1+w_2)$ to 1 when the complexity of the surrounding geometry goes from very high to very low. The overall CF of the PV plant is simply the multiplication of these three CFs: $\mathrm{CF} = \mathrm{CF}_i \times \mathrm{CF}_\eta \times \mathrm{CF}_g$. A keen reader would notice that the ratio introduced in (26) can indeed be used to assess and compare the sunlight access in different cities or different parts of cities, as long as their geometrical information is available, for instance, via LiDAR data.

VI. Application of the Presented Mathematical Framework in Urban Solar Electricity Prediction

Being consistently cheaper than other energy technologies, supported by policies and maturing technologies, solar PV is spreading worldwide [45]. The tendency is to put production and demand very close to each other, leading to massive PV integration in urban areas [46], [47]. A few fundamental issues arise when PV is massively deployed in rough geometries, i.e., urban areas:

1) prediction of PV power under shading caused by rough geometry and raised horizon [11], [21];
2) privacy issues regarding the specification and power production by each PV system [48];
3) impact on the electrical grid [28].

Due to privacy issues, it is hardly possible to share PV systems' monitored power production with a local network operator. On the other hand, prediction is not that simple because PV systems are placed under conditions that are frequently shaded. Now that the number of PV systems in urban areas is increasing, their influence on the grid is also increasing, and in many cases, the power from PV must be curtailed due to a lack of knowledge about accurate forecasts, lack of storage, or low capacity of the grid.

To put our mathematical framework to the test, anonymous data from a fleet of PV systems in the city of Eindhoven, provided kindly by Solar Monkey B.V., are used. Two regions in Eindhoven are selected: one in the city center and other in the countryside, respectively, shown by red and blue boxes in Fig. 8. In each region, 50 PV systems are randomly selected, and the energy yield of the two fleets is predicted using our mathematical framework and compared with real measurements. The only information from the systems is the aggregated installed capacity of each fleet, respectively, 198.6 and 278.1 kWp for the urban and countryside. Exact installation spot or orientation of the systems is unknown, thus respecting the privacy of the owners. Every piece of information that is given from the PV systems, in the form of a fleet, not an individual system, can still maintain the owners' privacy but make the probabilistic prediction more precise. For example, if it is known that the systems have tilt angles between μ_1 and μ_2 and are installed on building heights of z_1 to z_2. Knowing this information, one can formulate a more precise equation for $S(\theta)$ as

$$\begin{aligned} S(\theta)\,|_{\mu_1<q_0<\mu_2, z_1<z_0<z_2} &= \int_{-\infty}^{+\infty} dz_0 \int_{-\infty}^{+\infty} dp_0 \int_{-\infty}^{+\infty} dq_0 S(z_0, p_0, q_0, \theta) \\ &\quad \times f'_Z(z_0) f'_P(p_0) f'_Q(q_0) \end{aligned} \tag{27}$$

where $f_Q'(q_0)$, $f_P'(p_0)$, and $f_Z'(z_0)$ are modified distribution functions that are obtained by knowing the limits of slope and height (that the PV systems are installed within), through

$$f'_X(x) = \begin{cases} f_X(x)/\left(F_X(x=x_2) - F_X(x=x_1)\right) & x_1 < x < x_2 \\ 0, & \text{else} \end{cases}. \tag{28}$$

Therefore, $S(\theta)$ can be written further as

$$\begin{aligned} S(\theta)\,|_{\mu_1<q_0<\mu_2, z_1<z_0<z_2} &= \left[\int_{\mu_1}^{\mu_2} h(\mu - q_0) f_Q(q_0) dq_0\right] \\ &\quad \times \left(\frac{1}{\Lambda(\mu)+1}\right) \\ &\quad \frac{\left((F_Z(z_0=z_2))^{\Lambda(\mu)+1} - (F_Z(z_0=z_1))^{\Lambda(\mu)+1}\right)}{\left(F_Q(q_0=\mu_2) - F_Q(q_0=\mu_1)\right)\left(F_Z(z_0=z_2) - F_Z(z_0=z_1)\right)}. \end{aligned} \tag{29}$$

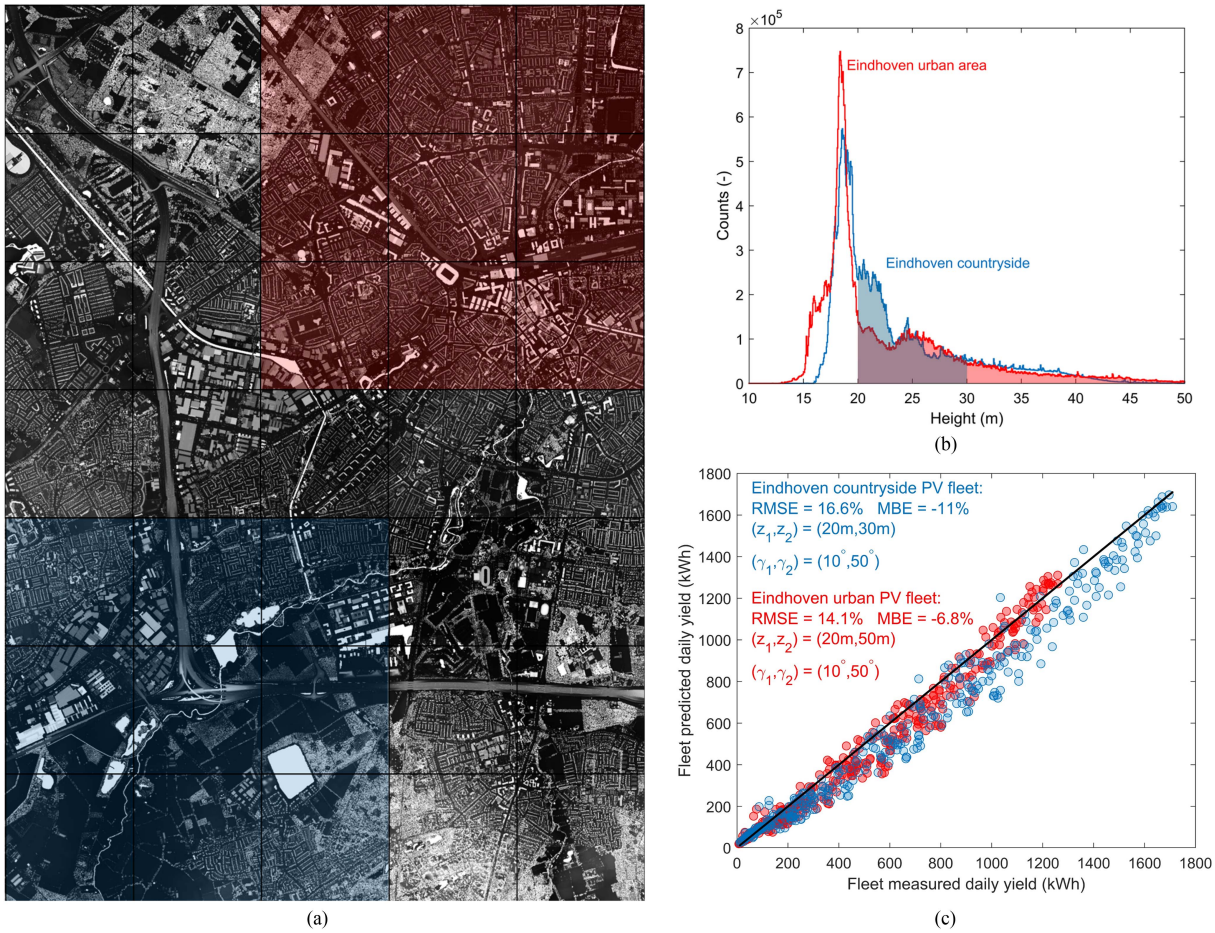

Fig. 8. Probabilistic PV fleet yield prediction and comparison with Solar Monkey B.V. data. (a) DSM of Eindhoven. The exact location of the PV systems is not known. Only the areas in which they are located are highlighted: blue for the village group and red for the urban group. There are 50 systems in each group. (b) Histograms of height count that portray the height distribution in the two regions of Eindhoven. The water points are removed from the counts because LiDAR data associated with the water areas are noisy due to water reflections. The assumed height ranges for PV system installation in both regions are highlighted. (c) Predicted versus measured daily yield of the two fleets. The percentage mean bias and RMSEs are shown in the figure. The results were obtained with hourly resolution but presented with daily resolution on the graph. The black line shows the perfect prediction, where measurement and prediction are the same.

It is noted that for $z_1 = \mu_1 = -\infty$ and $z_2 = \mu_2 = \infty$, this equation turns into (12). Having this more pertinent $S(\theta)$ equation at hand, (24) can be used to predict the PV fleet power. Fig. 8 shows the comparison between probabilistic prediction and measured values for the two PV fleets in Eindhoven. The PV systems were installed with tilt angles between 10° and 50°; thus, $\mu_1 = -\cot(90 - 50)$ and $\mu_2 = -\cot(90 - 10)$. No information was given about the systems' installation height; therefore, educated guesses were made for the height range in the urban and countryside areas of Eindhoven. Eindhoven is 16 m above sea level, and since no PV system is installed on the ground and all of them are on rooftops, it is assumed that $z_1 = 20$ m and $z_2 = 50$ m for the urban area (roughly one- to nine-storey buildings) and $z_1 = 20$ m and $z_2 = 30$ m (roughly one- to three-storey buildings) for the countryside. Fig. 8(b) plots the distribution of heights in the two regions of study, while Fig. 8(c) shows the comparison between measured and predicted yields every day.

As can be seen in Fig. 8, the probabilistic approach predicts the PV system yields with good accuracy most of the year, but on average, it underestimates. It is indeed expected because the PV systems' location is usually cherry picked, while the probabilistic approach assumes a random distribution over the city. The systems are mainly due South, but the probabilistic approach gives equal possibility to all orientations. As increasingly PV systems are installed and more areas are covered in the city by PV elements, the accuracy of the probabilistic approach increases as well. This is the same principle as for any other probability experiment, in which by increasing the number of trials (i.e., PV system populations in the fleet), the outcome (i.e., predicted yield) becomes more precise. The inaccuracy of the irradiance decomposition model could potentially contribute to the errors as well.

Using such a prediction approach, grid operators can conveniently calculate the expected power from PV fleets in different regions of urban areas and thus apply sufficient, not too low not too much, grid re-enforcements. The described approach can also have applications in power predictions and storage sizing when combined with irradiance prediction methods. When the next time step irradiance is predicted, it can be plugged into the aforementioned mathematical formulation to predict the PV power, without the need for lengthy simulations. The current

framework can also be used to assess bifacial PV systems, as they are increasingly used in urban areas. The performance of bifacial PV modules is tightly linked with albedo, which is, among others, a function of shadowing distribution on an area [49]. The neighborhoods with a higher chance of being shaded—lower $S(\theta)$—will have lower bifacial PV gain.

VII. Overview and Outlook

A. Overview

The importance of sunlight in our daily life in urban areas is ever-increasing. On the one hand, sunlight supports health and mental indicators. On the other hand, it provides input for clean electricity production through PV and/or thermal power conversion. While sunlight remains the key input, the geometry of urban environments defines the relationship between sunlight and the demand side. This important link between geometry and sunlight needs to be understood well, which facilitates informed decision making and planning in urban contexts. Realizing the significance of this need, in this research, the Wagner–Smith shadowing theory for rough surfaces was first extended, and a set of equations [see (5) and (6)] that gives the illumination chance of a surface within a rough geometry was obtained. The specific cases of this formulation [see (7)–(10)] were discussed, and it was shown that the formulation works for any distribution of heights and slopes, as long as they remain independent. A great advantage is that the presented formulation can be expressed in the form of CDFs of heights and slopes, which makes it extremely trivial to implement (whether CDFs are at hand analytically or numerically) as well as understand.

Furthermore, a PMF, a discrete form of the PDF, of expected sunlight energy falling on a group of surfaces in a rough geometry was obtained. This was done because of multiple reasons. First, there were reports in the literature that PV-integrated surfaces, whether fixed (building-integrated PV) or moving (vehicle-integrated PV), show some sort of probability distribution when their specific energy (kWh/kWp) is assessed in large numbers. However, the underlying understanding that could generalize such probability distributions was lacking. The second reason was the privacy concerns that usually arise when detailed information from PV systems owners is needed to assess or monitor rooftop PV performance. While they are studied as ensembles, not individuals, such concerns can be addressed. The third reason was the enormous potential use cases for other fields of science, as PDFs are widely in use in science and engineering fields, thus opening opportunities for future applications.

While looking into the PMF for expected sunlight energy, the necessity for an enclosed formula for the SVF in rough geometry was recognized. This was needed primarily to enable fast diffuse sunlight calculation, but when the equation was found (17), another avenue of application was unlocked, where one can use the SVF equation in urban heat island studies, geography, relief visualizations, etc.

Our next step was the parametrical investigation of the PMF. It was shown how its shape alters depending on the geometrical roughness of the surface and presented its application with a more sensible yet hypothetical example of rooftop PV fleets in different regions of Delft. Interestingly, it was observed how the electrical CF of a PV fleet is a function of urban geometry. Finally, LiDAR data and measured PV system yields in Eindhoven were used to show the reliability of the obtained PMF, and it was demonstrated how it can be used to predict the electricity output of PV fleets with limited information and no privacy violation. This is of great importance for grid congestion studies.

B. Outlook

Fast urbanization and the high population density of urban dwellers have limited access to sunlight energy while boosting the demand for clean electricity [50]. Moreover, implementing PV technology on all possible surfaces around us [44] requires a thorough understanding of sunlight interaction with geometrical features of urban areas. In such situations, it is crucial not only to assess the sunlight access but also to understand how it is linked with the geometry of the city, quantitatively. No matter if the surfaces of interest are PV cells or human skin, as long as they are studied as an ensemble, the described mathematical framework in this work can be utilized to obtain the PMF of the sunlight energy on those surfaces. An important feature of the presented framework is that it can be tailored to specific target surfaces in urban areas, through (27), as long as they can be characterized with p_0, q_0, and z_0 ranges. For instance, all the south-to-east vertical facades in a neighborhood, horizontal pedestrian walk paths, etc. It is noted that although the focus was mainly on urban areas and solar PV to demonstrate the applications of the proposed methodology, it mathematically holds for other geometrical sizes as long as it remains bigger than the wavelength of interacting light so that the rectilinear property of light can be used. This means possible applications in other fields, such as material science and texture engineering. Overall, the presented framework can contribute to answering impactful questions such as "*How much sunlight access do pedestrians get in a certain area of a city*," "*Which parts of a city are more prone to heat accumulation*," "*Where does the electrical grid need enforcement to avoid congestions issues*," "*What is the angular dependency of a specific surface texturing*," and so on. The low input demand and the framework simplicity make it suitable for vast applications, ranging from urban health concerns to electrical grid congestion problems. However, its key contribution is that it helps understand better the relation between energy and geometry in a rough surface context.

Acknowledgment

The author would like to thank Rohi Perlsteyn, from Solar Monkey B.V., for kindly supporting the validation part of this research by providing anonymous solar photovoltaic monitored yield in the region of Eindhoven, The Netherlands. The author also appreciates Yilong Zhou's kind support in downloading and preprocessing LiDAR data of The Netherlands and the United States.

References

[1] P. E. Glaser, "Power from the sun: Its future," *Science*, vol. 162, no. 3856, pp. 857–861, 1968.

[2] R. Mackey, "Rhodes fairbridge and the idea that the solar system regulates the earth's climate," *J. Coastal Res.*, vol. 50, pp. 955–968, 2024.

[3] United Nations, D.O.E and P.D. Social Affairs, *World Population Prospects 2022: Ten Key Messages*. New York, NY, USA: United Nations, 2022.

[4] S. Malekpour et al., "What scientists need to do to accelerate progress on the SDGs," *Nature*, vol. 621, no. 7978, pp. 250–254, 2023.

[5] A. C. Burns et al., "Day and night light exposure are associated with psychiatric disorders: An objective light study in>85,000 people," *Nat. Ment. Health*, vol. 1, no. 11, pp. 853–862, 2023.

[6] T. Weil et al., "Daily changes in light influence mood via inhibitory networks within the thalamic perihabenular nucleus," *Sci. Adv.*, vol. 8, no. 23, 2022, Art. no. eabn3567.

[7] H. Zhu et al., "Moderate UV exposure enhances learning and memory by promoting a novel glutamate biosynthetic pathway in the brain," *Cell*, vol. 173, no. 7, pp. 1716–1727, 2018.

[8] H. Li, F. Cui, T. Wang, W. Wang, and D. Zhang, "The impact of sunlight exposure on brain structural markers in the UK biobank," *Sci. Rep.*, vol. 14, no. 1, 2024, Art. no. 10313.

[9] S. Sen and L. Khazanovich, "Limited application of reflective surfaces can mitigate urban heat pollution," *Nat. Commun.*, vol. 12, no. 1, 2021, Art. no. 3491.

[10] X. Huang, E. Bou-Zeid, I. Pigliautile, A. L. Pisello, and J. Mandal, "Optimizing retro-reflective surfaces to untrap radiation and cool cities," *Nat. Cities*, vol. 1, no. 4, pp. 275–285, 2024.

[11] T. N. de Vries et al., "A quick-scan method to assess photovoltaic rooftop potential based on aerial imagery and LiDAR," *Sol. Energy*, vol. 209, pp. 96–107, 2020.

[12] K. M. Zielinska-Dabkowska and K. Xavia, "Protect our right to light," *Nature*, vol. 568, no. 7753, pp. 451–453, 2019.

[13] J. Lin, J. Ma, and J. Zhu, "A privacy-preserving federated learning method for probabilistic community-level behind-the-meter solar generation disaggregation," *IEEE Trans. Smart Grid*, vol. 13, no. 1, pp. 268–279, Jan. 2022.

[14] Y. Zhou, M. Verkou, M. Zeman, H. Ziar, and O. Isabella, "A comprehensive workflow for high resolution 3D solar photovoltaic potential mapping in dense urban environment: A case study on campus of Delft University of Technology," *Sol. RRL*, vol. 6, no. 5, 2022, Art. no. 2100478.

[15] S. Freitas, C. Catita, P. Redweik, and M. C. Brito, "Modelling solar potential in the urban environment: State-of-the-art review," *Renewable Sustain. Energy Rev.*, vol. 41, pp. 915–931, 2015.

[16] A. Palliwal, S. Song, H. T. W. Tan, and F. Biljecki, "3D city models for urban farming site identification in buildings," *Comput., Environ. Urban Syst.*, vol. 86, 2021, Art. no. 101584.

[17] C. Chatzipoulka, R. Compagnon, and M. Nikolopoulou, "Urban geometry and solar availability on façades and ground of real urban forms: Using London as a case study," *Sol. Energy*, vol. 138, pp. 53–66, 2016.

[18] E. Andreou, "The effect of urban layout, street geometry and orientation on shading conditions in urban canyons in the Mediterranean," *Renewable Energy*, vol. 63, pp. 587–596, 2014.

[19] Y. Zhou, D. Wilmink, M. Zeman, O. Isabella, and H. Ziar, "A geographic information system-based large scale visibility assessment tool for multi-criteria photovoltaic planning on urban building roofs," *Renewable Sustain. Energy Rev.*, vol. 188, 2023, Art. no. 113885.

[20] K. H. Poon, J. H. Kämpf, S. E. R. Tay, N. H. Wong, and T. G. Reindl, "Parametric study of URBAN morphology on building solar energy potential in Singapore context," *Urban Climate*, vol. 33, 2020, Art. no. 100624.

[21] A. Calcabrini, H. Ziar, O. Isabella, and M. Zeman, "A simplified skyline-based method for estimating the annual solar energy potential in urban environments," *Nat. Energy*, vol. 4, no. 3, pp. 206–215, 2019.

[22] H. Lan, Z. Gou, and X. Xie, "A simplified evaluation method of rooftop solar energy potential based on image semantic segmentation of urban streetscapes," *Sol. Energy*, vol. 230, pp. 912–924, 2021.

[23] H. Lan, Z. Gou, and C. Hou, "Understanding the relationship between urban morphology and solar potential in mixed-use neighborhoods using machine learning algorithms," *Sustain. Cities Soc.*, vol. 87, 2022, Art. no. 104225.

[24] A. Vartholomaios, "A machine learning approach to modelling solar irradiation of urban and terrain 3D models," *Comput., Environ. Urban Syst.*, vol. 78, 2019, Art. no. 101387.

[25] C.-B. Hu, F. Zhang, F.-Y. Gong, C. Ratti, and X. Li, "Classification and mapping of urban canyon geometry using Google street view images and deep multitask learning," *Building Environ.*, vol. 167, 2020, Art. no. 106424.

[26] S. Chang, N. Saha, D. Castro-Lacouture, and P. P.-J. Yang, "Generative design and performance modeling for relationships between urban built forms, sky opening, solar radiation and energy," *Energy Procedia*, vol. 158, pp. 3994–4002, 2019.

[27] R. Lazdins, A. Mutule, and D. Zalostiba, "PV energy communities—Challenges and barriers from a consumer perspective: A literature review," *Energies*, vol. 14, no. 16, 2021, Art. no. 4873.

[28] A. T. Procopiou and L. F. Ochoa, "Asset congestion and voltage management in large-scale MV-LV networks with solar PV," *IEEE Trans. Power Syst.*, vol. 36, no. 5, pp. 4018–4027, Sep. 2021.

[29] *Communications With Daan van Es, Data Analyst at Alliander (Dutch Unitility Company and Network Operator)*, Jun. 13 2024.

[30] R. Wagner, "Shadowing of randomly rough surfaces," *J. Acoust. Soc. Amer.*, vol. 41, no. 1, pp. 138–147, 1967.

[31] B. Smith, "Geometrical shadowing of a random rough surface," *IEEE Trans. Antennas Propag.*, vol. AP-15, no. 5, pp. 668–671, Sep. 1967.

[32] G. Brown, "Shadowing by non-Gaussian random surfaces," *IEEE Trans. Antennas Propag.*, vol. AP-28, no. 6, pp. 788–790, Nov. 1980.

[33] C. Bourlier, G. Berginc, and J. Saillard, "One-and two-dimensional shadowing functions for any height and slope stationary uncorrelated surface in the monostatic and bistatic configurations," *IEEE Trans. Antennas Propag.*, vol. 50, no. 3, pp. 312–324, Mar. 2002.

[34] Datasets - PDOK. Accessed: Jan. 2024. [Online]. Available: https://www.pdok.nl/datasets

[35] F. F. Sönmez, H. Ziar, O. Isabella, and M. Zeman, "Fast and accurate ray-casting-based view factor estimation method for complex geometries," *Sol. Energy Mater. Sol. Cells*, vol. 200, 2019, Art. no. 109934.

[36] A. Middel, J. Lukasczyk, R. Maciejewski, M. Demuzere, and M. Roth, "Sky view factor footprints for urban climate modeling," *Urban Climate*, vol. 25, pp. 120–134, 2018.

[37] D. Steyn, "The calculation of view factors from fisheye-lens photographs: Research note," *Atmos.-Ocean*, vol. 18, pp. 254–258, 1980.

[38] M. Keijzer, "A multi-surface reflected irradiance model for pyranometer corrections and PV yield calculations in complex urban geometries," M.Sc. thesis, Elect. Sustain. Energy Dept., Delft Univ. Technol., Delft, The Netherlands, 2019.

[39] C. Ferri et al., "Mapping the photovoltaic potential of the roads including the effect of traffic," *Renewable Energy*, vol. 182, pp. 427–442, 2022.

[40] U.S. Geological Survey—3DEP LidarExplorer Portal, Accessed: Feb. 2025. [Online]. Available: https://apps.nationalmap.gov/lidar-explorer/#/

[41] J. Taylor et al., "Performance of distributed PV in the U.K.: A statistical analysis of over 7000 systems," in *Proc. 31st Eur. Photovolt. Sol. Energy Conf. Exhib.*, 2015, pp. 2263–2268.

[42] D. de Jong and H. Ziar, "Photovoltaic potential of the Dutch inland shipping fleet: An experimentally validated method to simulate the power series from vessel-integrated photovoltaics," *Sol. RRL*, vol. 7, no. 8, 2023, Art. no. 2200642.

[43] V. Sionti, "Photovoltaic potential of the fleet of urban vehicles," M.Sc. thesis, Elect. Sustain. Energy Dept., Delft Univ. Technol., Delft, The Netherlands, 2021.

[44] H. Ziar, "The photovoltaic potential of a fleet of urban vehicles: Potential and challenges for PV everywhere! plenary," in *Proc. 8th World Conf. Photovolt. Energy Convers.*, Milan, Italy, 2022, pp. 1–6.

[45] World Energy Outlook 2023, *Licence: CC BY 4.0 (Report); CC BY NC SA 4.0 (Annex A)*, Int. Energy Agency, Paris, France, 2023. [Online]. Available: https://www.iea.org/reports/world-energy-outlook-2023

[46] A. Strzalka, N. Alam, E. Duminil, V. Coors, and U. Eicker, "Large scale integration of photovoltaics in cities," *Appl. Energy*, vol. 93, pp. 413–421, 2012.

[47] V. Kapsalis et al., "Critical assessment of large-scale rooftop photovoltaics deployment in the global urban environment," *Renewable Sustain. Energy Rev.*, vol. 189, 2024, Art. no. 114005.

[48] S. Heuninckx, M. Meitern, G. te Boveldt, and T. Coosemans, "Practical problems before privacy concerns: How European energy community initiatives struggle with data collection," *Energy Res. Social Sci.*, vol. 98, 2023, Art. no. 103040.

[49] H. Ziar, F. F. Sönmez, O. Isabella, and M. Zeman, "A comprehensive albedo model for solar energy applications: Geometric spectral albedo," *Appl. Energy*, vol. 255, 2019, Art. no. 113867.

[50] D. M. Kammen and D. A. Sunter, "City-integrated renewable energy for urban sustainability," *Science*, vol. 352, no. 6288, pp. 922–928, 2016.